On the noise reduction mechanism of over-tip liners

Ramesh Raja Subramanyam,[1] Suresh Palani,[1] Chaitanya Paruchuri,[1] and Sergi Palleja-Cabre[1]

Institute of Sound and Vibration, University of Southampton, Southampton, Hampshire, SO17 1BJ, United Kingdom

(Dated: 18 January 2024)

The application of acoustic liners near/directly over a sound source has gained significant interest for the excess noise reduction achieved with Over-the-Rotor (OTR) liners compared to the conventional liner installations at the intake of an aero-engine. However, the mechanism of noise reduction achieved in the OTR liners is not clearly understood. This paper aims to explain this mechanism by considering a static monopole source placed over a finite liner insert with a zero background mean flow. This has been investigated numerically using COMSOL Multiphysics in a half-space domain and compared with reference analytical solutions for infinite lined walls. One of the key findings of the paper is the underlying physics of the source modification mechanism, which has been found to be the interference between the primary noise source and a secondary noise source forming on the liner surface. It is identified through an optimal impedance study that this back-reaction mechanism is dominant when the source is located for a normalised tip gap, $e/\lambda < 0.25$, where e is the distance between the source and the liner surface and λ is the acoustic wavelength. Within this region, there exists an optimum normalised liner length, L/e providing a maximum insertion loss.

I. INTRODUCTION

Liners are passive noise reduction treatments used across different industrial sectors. In aero-engines, liners are conventionally placed in the intake and bypass region of turbofan engines. Due to the increase in the bypass ratio and the reduction in the length of the engines, the effective lined area in the engine has reduced. In addition, the predicted growth of air travel will require further reductions in engine noise to meet regulations. The use of liners in the vicinity of the rotor has been studied extensively in recent times to further increase noise suppression. This liner configuration is particularly suited to reducing the acoustic signature of urban air mobility vehicles with compact noise propulsion systems like shrouded propellers. More generally, this technology can be used to reduce noise in any application involving ducted rotors, not only in aerospace but also in the automotive industry and for heating, cooling and ventilation systems.

Some of the first studies of Over-The-Rotor (OTR) liners were carried out with Foam Metal Liners (FML) as they had a small impact on the performance of the engine and are compatible with a wide range of operating conditions (Jones *et al.*, 2009; Sutliff *et al.*, 2008). FML were designed with various values of porosity and thickness and tested in an OTR configuration in the low-speed fan ANCF testbed at NASA GRC by Sutliff and Jones (Sutliff and Jones, 2009). The far-field noise was measured with a semi-circular array of microphones around the exhaust and the surface pressure was measured at five points over the FML. An insertion loss of 5 dB in far-field noise was observed, which was attributed to the effect of source modification and conventional attenuation. Further testing of OTR liners by Sutliff et al. (Sutliff *et al.*, 2009) using a high-speed fan showed that the OTR liners were effectively reducing the noise only up to sonic tip speed. The effect of OTR liners on the performance of the engine was evaluated by Bozak et al. (Bozak *et al.*, 2013). It was shown that OTR configurations with circumferential grooves have minimal impact on the aero-engine performance.

In the above literature, the main reason for the effectiveness of OTR liners was attributed to the noise reduction in the near field region of the rotor by acting as a pressure release boundary condition. This problem was studied analytically in (Palleja-Cabre *et al.*, 2022b) by coupling the fan sources, represented by a point source, with the sound propagation and noise suppression by using Green's functions and mode-matching techniques. It was found that the source modification effects for the values of impedance investigated were most dominant for $e/\lambda < 0.5$, where e is the distance from the source to the liner wall and λ is the acoustic wavelength. This model was improved in (Palleja-Cabre *et al.*, 2022a) to include the modelling of an inlet termination and distributed rotating sources and compared with the experimental results of Bozak and Dougherty (Bozak and Dougherty, 2018). More recently, this problem was also studied analytically by Sun et al. (Sun *et al.*, 2022) by using a coupled singularity method. It was found that the OTR liners can alleviate the unsteady blade loading and that the close proximity to the fan intensifies the fluid particle oscillation through the acoustically treated wall.

Further experimental work was performed by Palleja-Cabre et al.(Palleja-Cabre *et al.*, 2020) by using a simplified set-up in which the fan rotor and OTR liner were represented by a static airfoil with its tip located over a flat plate containing the liner insert. It was found that the noise reduction in the region close to the liner is independent of the flow speed but it decreased with the increase in the tip gap. The balance of the source modification and conventional attenuation effects was studied with different types of liner inserts but the results were inconclusive. The experimental results were also compared to analytical predictions based on an adaptation of the work of Thomasson (Thomasson, 1976) and Levine (Levine, 1980) for a point source over a lined plane. It was assumed that the sources of tip leakage noise are concentrated at the aerofoil tip and that they can be approximated as a point source over a rigid or lined infinite plane. The model was found to have a qualitative agreement with experimental results. However, it was hypothesised in the literature that the aerodynamic effects of the liners in the tip gap region are also influencing the measured far field noise. This motivated the current numerical analysis of the problem to distinguish the acoustic source modifications and aerodynamic modifications due to a different tip leakage flow.

This work is an extension of the study of using the liners in the near field or in proximity to the sound source. The primary objective of the present work is to improve the understanding of the physical noise reduction mechanism of placing liners close to a sound source and trying to isolate them in the absence of flow. The key contributions of this research are:

- Description of the physical mechanism of the back reaction effects observed with liners located near the point source, and showing that this effect is dominant for $e/\lambda < 0.25$.
- The dependency of the optimal impedance on the tip gap, e, the liner length, L, and the acoustic wavelength, λ, and the effect of these parameters in the total noise reduction achieved with the liners located near the point source.

II. COMPUTATIONAL MODEL

A. Analytical optimal impedance study

An optimal impedance study was first performed analytically to see the dependency of the impedance on the tip gap, e. In the Ingard and Lamb (Ingard, 1951) analytical models, the reflections due to the proximity of the sound source to the boundary were considered to be the effect of an image source. This image source modifies the total radiated sound power level in the far field, which can be obtained by integrating the energy flux in the far field over the half-space. The acoustic power is then normalised by the free field power or the sound power generated in the absence of a boundary at a similar distance. The ratio of those is used to determine a power amplification factor. The power amplification factor for a monopole source over a hard wall is expressed as,

$$\frac{P}{P_f} = 1 + \frac{\sin z}{z}, \tag{1}$$

and for a dipole,

$$\frac{P}{P_f} = 1 + \frac{3}{z}\left[\frac{\sin z}{z^2} - \frac{\cos z}{z}\right], \tag{2}$$

where, P is the power in the half space domain, P_f is the power in the free field, and $z = 2ke$, with k representing the wavenumber and e being the tip gap.

Thomasson (Thomasson, 1976) extended the Ingard model for the infinitely lined boundary and Levine (Levine, 1980) provided closed-form analytical expressions of the power amplification factors for a monopole point source in such conditions. These are calculated for the lined boundary as given below.

$$\frac{P}{P_f} = 1 + \frac{\sin z}{z} + 2\,\mathrm{Re}(Ae^{jAz}[E_1(j[1+A]z) - E_1(jAz)]) - 2\,\mathrm{Re}(A)\int_0^1 \frac{\mu.d\mu}{\left|A + \sqrt{1-\mu^2}\right|^2}, \quad (3)$$

where

$$E_1(\zeta) = \int_\zeta^\infty \frac{x^{-\xi}d\xi}{\xi}, |arg(\zeta)| < \Pi, \quad (4)$$

A is the admittance, and ζ and μ are dummy variables. The admittance in Equation 3 is the inverse of the acoustic impedance of the liner, Z.

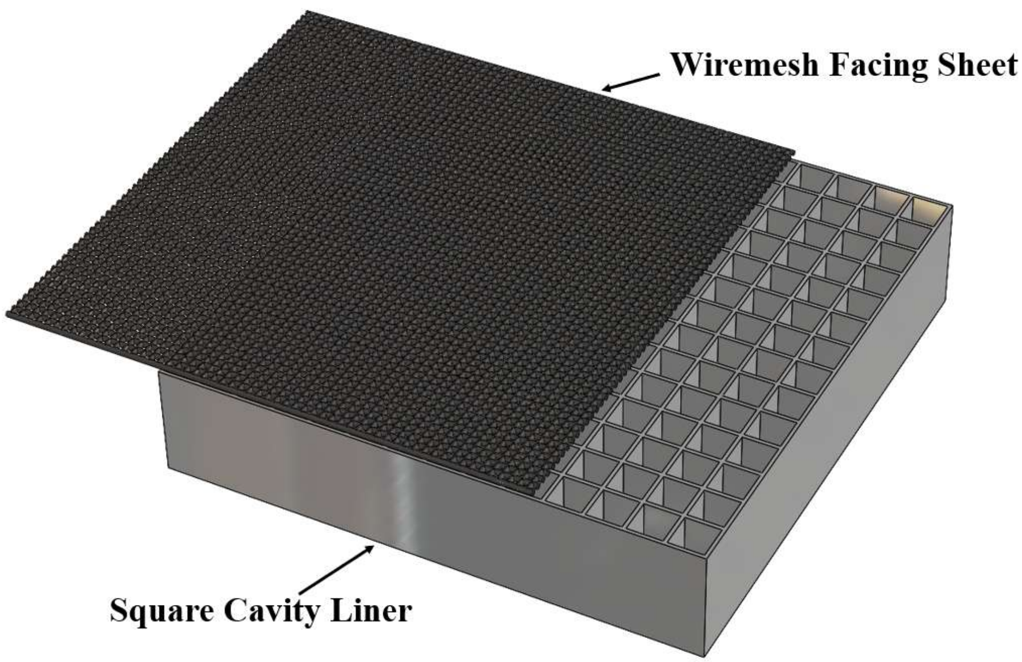

FIG. 1: Single Degree of Freedom liner with wire-mesh facing sheet.

Figure 1 shows a Single Degree of Freedom (SDOF) liner with a wire-mesh facing sheet, which has been used for most of the analysis in this paper. The properties of the liner that was used for the experimental study reported in the later section of this manuscript were given as the input to the numerical model. The cavity depth of the SDOF liner, h, is set to 30.48 mm. Liner samples were tested experimentally in a normal incidence impedance tube. The inertance of the wire-mesh was estimated through the application of a total reactance fit to the measured data (see Figure 2). As expected, the estimated inertance was very small, typical for a wire-mesh facing sheet, and was assumed to be a constant value of 8 mm. The predicted normalised resistance, normalised reactance, and absorption coefficient spectra for the liner used in this study were compared with the measured data and shown in Figure 2. The measurement is valid for frequencies between 0.1 and 5 kHz due to the length and diameter of the impedance meter. The normalised resistance R is assumed to be a constant at 1ρc across all frequencies as it is a linear liner. The reactance is calculated by adding the mass reactance kM_f and the cavity reactance, which is a function of wavenumber k and cavity depth h as shown in Equation 5. As shown in Figure 2, the liner was found to be in resonance at 2250 Hz which is signified by the zero reactance and maximum absorption of $\alpha = 1$. The second resonance of the liner is approximately at 7000 Hz. The anti - resonance condition was present in frequencies close to 200 Hz and 5600 Hz, corresponding to the point where the impedance becomes infinite causing the absorption coefficient to be zero. For most of the analysis in this paper, the noise source was generated at these resonance and anti-resonance frequencies to study the noise reduction mechanism of the liner for the over-the-rotor application.

$$Z \; = \; R \; + \; i \, [k \; M_f \; - \; cot(kh)] \tag{5}$$

The analytical optimal impedance is determined by varying the resistance and reactance at 2250 Hz resonance frequency. The resistance values were varied from 0 to 5 in steps of 0.05

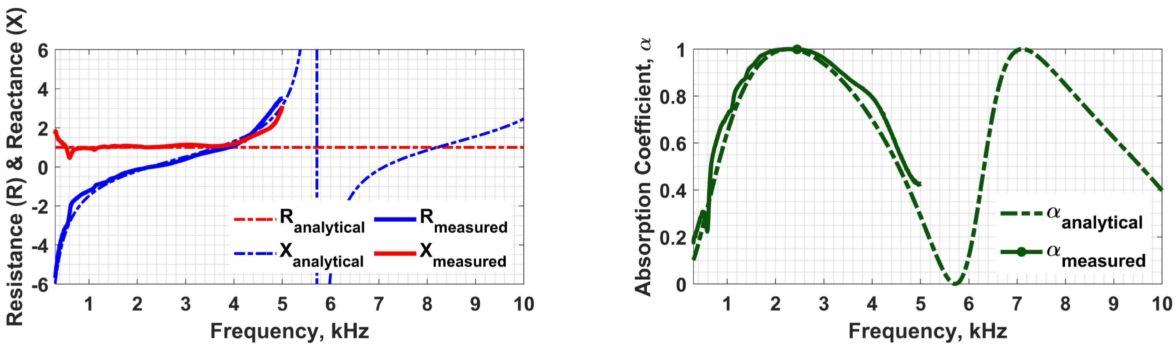

(a) (b)

FIG. 2: (a) Resistance and Reactance plot of the liner (b) Absorption spectra of the liner.

while the reactance was varied from -5 to 5 with 0.05 resolution. The difference in radiated power between the lined and hardwall configurations, the insertion loss, is calculated for different tip gaps ranging from 0 m to 1.5 m by using the power amplification factors in the above equations. The resistance and the reactance that yield maximum insertion loss for each gap size are then determined. This is the optimal resistance and reactance for the given tip gap in the considered frequency. The optimal resistance and reactance are plotted against the tip gap normalized by the wavelength in Figure 3. The results obtained with the analytical model are shown by the solid lines and the optimal impedance calculated from the numerical model with a 9 m liner (longest liner in the considered domain) for different tip gaps is indicated by the markers.

The optimal resistance is observed to be close to zero up to $e/\lambda = 0.25$, indicated by the dashed line in Figure 3. When the resistance is zero, the particle velocity flow into the liner is high due to less damping on the facing sheet, which will be explained further in the results section. This value of e/λ is an important criterion for the back reaction effect and is one of the key findings in this work. The region to the left of this point can therefore be termed the region of back reaction as this is the dominant noise reduction mechanism. This point corresponds to a tip gap of 0.038 m for a monopole sound source producing a tone at 2250 Hz. Beyond this region, the noise reduction is progressively dominated by the conventional absorption of the liner and hence termed here as the region of absorption. Since the numerical model is developed to study the effects of a finite lined boundary, the values for the case with $L = 9$ m are shown only for comparison. The results and detailed analysis for the finite liner configurations are presented in later sections.

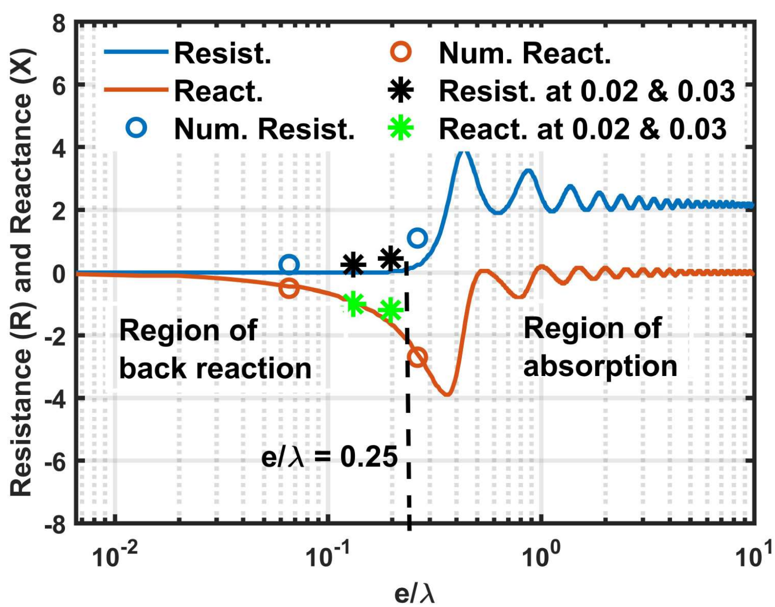

FIG. 3: Optimal resistance and optimal reactance for different tip gap at 2250 Hz.

The contour plots of the analytical optimal impedance for the selected tip gaps $e/\lambda = [0.065, 0.262, 0.459]$ m are shown in Figure 4 to visualise the variation in insertion loss with the tip gap. These values of tip gap were selected to represent the source location in the region of back reaction, at the transition point, and in the region of absorption. It can be interpreted from the figure that the peak insertion loss decreases with the increase in the tip gap signifying the reduction in the back reaction effect. The variation of optimal reactance with the tip gap indicates that the liner must be tuned for different tip gaps for maximum noise suppression at a given frequency. These results are however not directly comparable to the case of OTR liners since those are of finite length. Hence, the current numerical model was built to model the case of a finite liner.

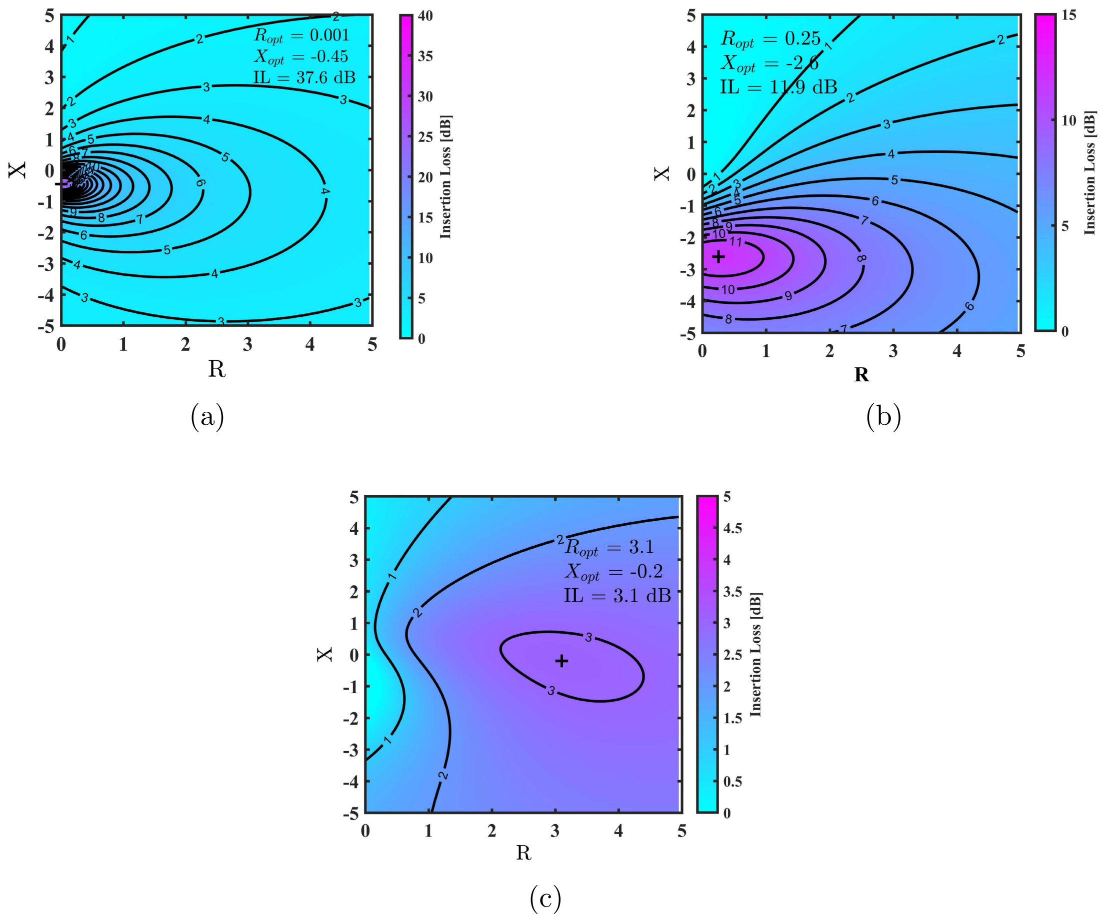

FIG. 4: Optimal impedance contour for infinite liner (a) $e/\lambda = 0.065$, (b) $e/\lambda = 0.262$, and (c) $e/\lambda = 0.459$.

B. Numerical COMSOL Model

The numerical model with a finite lined boundary was built in 2-D space in COMSOL. The 'Pressure Acoustics' physics was used, as it is a zero flow model, and the frequency domain study was performed. A semicircle of 5 metres radius was created and a monopole point source was initially positioned at a distance of 0.01 mm from the base of the semicircle. A Perfectly Matched Layer (PML) condition was given to the domain beyond the 5 metre arc. The monopole point source strength was kept at 50 m^2/s. In the base of the semicircle, the liner cavities were modelled and terminated by a hard wall on either side. It is essential to have a hardwall boundary between the PML boundary layer and the lined boundary condition in COMSOL. The maximum liner length was therefore limited to 9 m with 4.5 m on either side of the domain centre. The basic schematic of the model is shown in Figure 5. Figure 5 (a) depicts the back reaction and Figure 5 (b) shows the back scattering effect. The resistance and mass inertance of the facing sheet were given as a boundary condition and the cavity reactance was captured by physically modelling the cavity depth. This was done to investigate the particle velocity flow into the liner so as to understand the source modification mechanism. The initial conditions for the model are listed in Table I. The domains were mapped meshed with the element size varying from one-sixth to one-tenth of the wavelength of the maximum frequency. The model was solved by using the Helmholtz equation as given below,

$$\nabla . \left(-\frac{1}{\rho}(\nabla p_t + F_d) \right) - \frac{k^2}{\rho} p_t = Q_m, \tag{6}$$

where p_t is the total acoustic pressure in the domain, ρ is the density of the medium (air), k is the acoustic wavenumber, Q_m is the monopole source term, and F_d is the dipole source term.

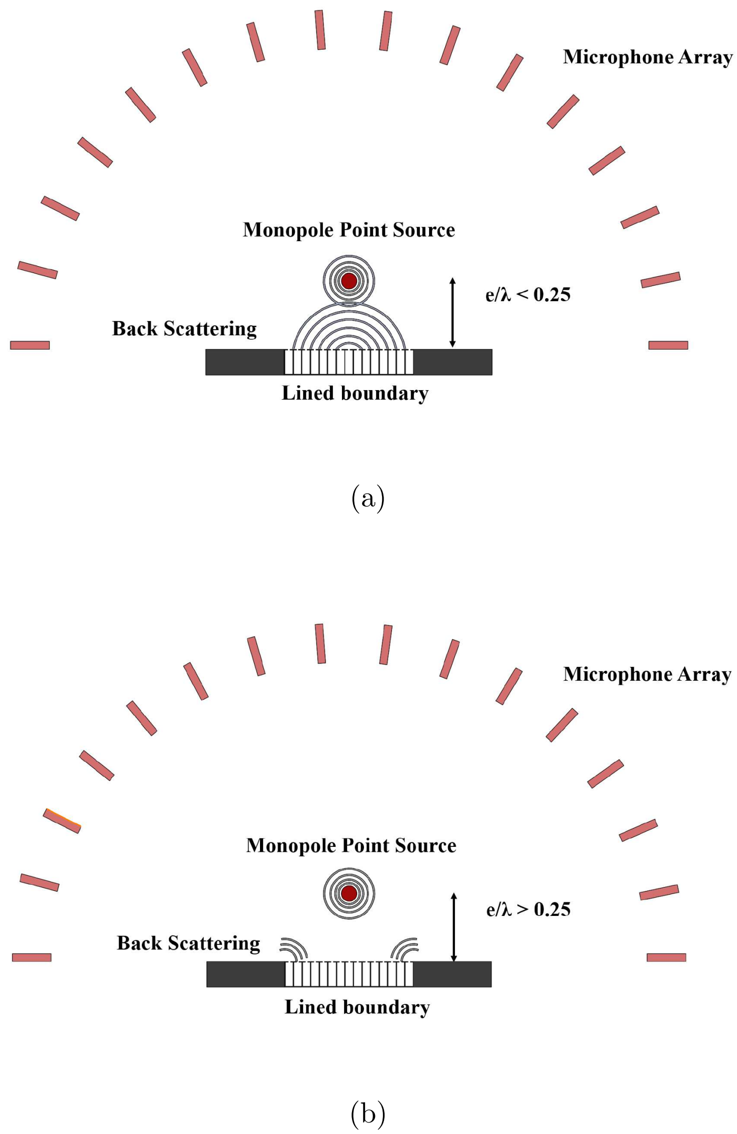

FIG. 5: (a) Schematic of the numerical model showing back reaction, (b) Schematic of the numerical model showing back scattering.

Geometry	Semicircular domain
Mean flow	Zero
Propagation	Linear
Impedance	Single degree of freedom, locally reacting, Normal impedance boundary condition
Source	static point source monopole and dipole
Measurement probes	Horizontal axis semicircular array microphones

TABLE I: Initial conditions in numerical model.

In line with the analytical model, the far field sound power is evaluated over a 4.5 m arc from the centre of the base. The far-field insertion loss is then calculated by subtracting the sound power for the hard wall and lined cases. The phase of the acoustic pressure and particle velocity flow into the liner are also evaluated to study the source modification mechanism. The latter was computed by taking the integral of the vertical particle velocity on top of each cavity.

C. Verification of the model

The model was initially verified for the hard wall boundary condition. The comparison of the power amplification factor between the numerical and the analytical model for the monopole and dipole source in the presence of the hardwall boundary is shown in Figure 6 (a) and (b) respectively. The power amplification factor was calculated for a fixed tip gap of

$e = 0.01\ mm$ while varying the frequency of the noise source. This was done to investigate the validity of the model across a range of frequencies. The model shows an agreement with the analytical predictions. There is a deviation of one decibel in the higher frequencies ($e/\lambda > 0.2$) due to the mesh size. The deviation was found to progressively reduce as we decreased the mesh size. The solution however was found to be converged for the mesh size utilised in this study.

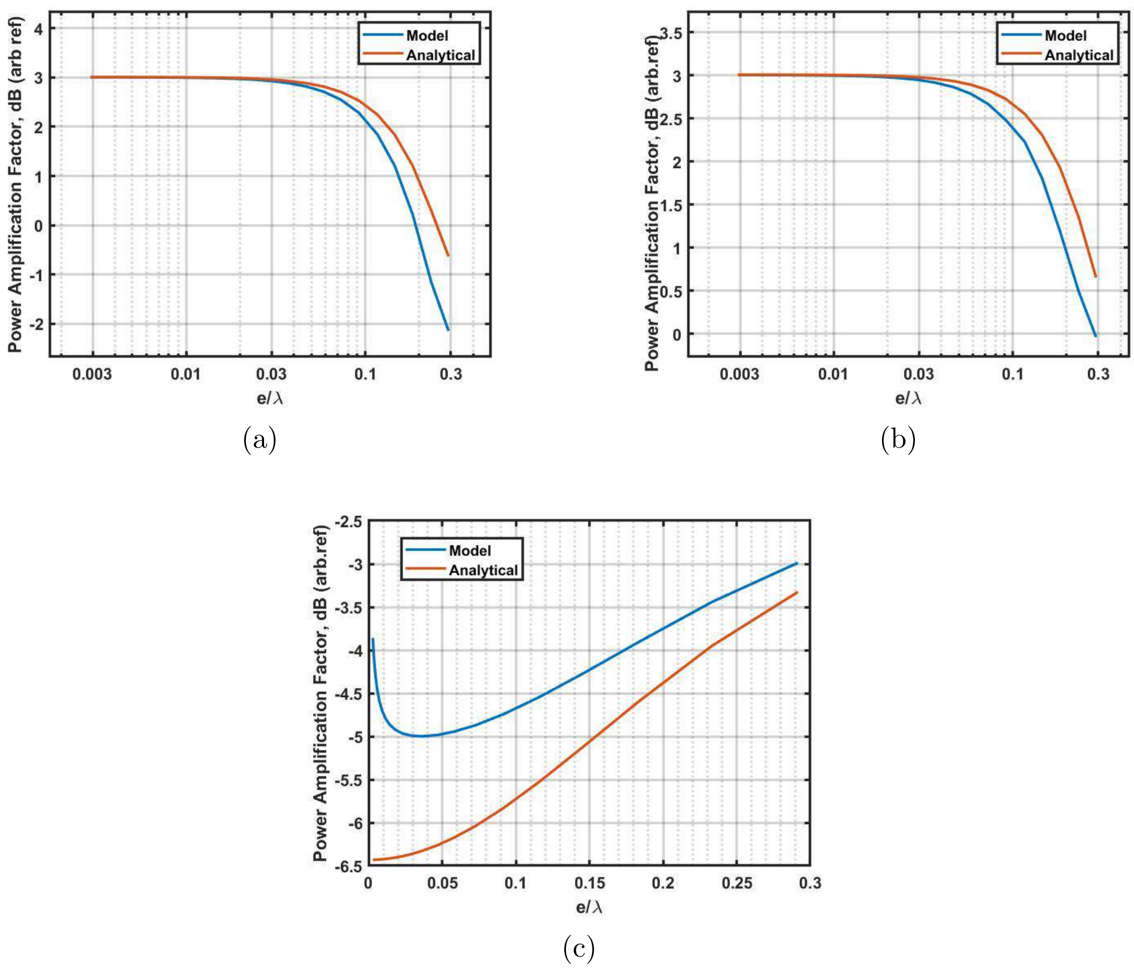

FIG. 6: Comparison of numerical and analytical model (a) Monopole source over a hard wall, (b) Dipole source over a hard wall, and (c) Monopole source over a lined wall.

The comparison of the power amplification factor for the lined boundary condition is shown in Figure 6 (c). The numerical model shows a similar qualitative behaviour to the analytical model. However, a deviation of 1 dB can be observed across all frequencies, which increases at the low frequency limit. This is attributed to the finite length of the liner considered in the model. It was suggested by Thomasson and Levine that the domain radius must be very large compared with the acoustic wavelength, but with the increase in the domain radius the mesh size had to be increased to reduce the computational load on the system. This introduced errors in the model and there were huge deviations due to that at high frequencies. The domain size was therefore kept at a 5 metre radius and the performance of the 9 m liner could not match with the analytical model perfectly. However, the same qualitative behaviour is observed in the numerical and analytical results, except for very low frequencies, the current model was used for further analysis.

III. RESULTS AND DISCUSSION

The results presented in this paper are categorised into three sections. A preliminary study of the various noise reduction mechanisms of the OTR liners is first presented. This study forms the basis for exploring the contributions from the back reaction and the back scattering effects due to OTR liners. The second section identifies the optimal impedance condition of OTR liners for achieving the maximum back reaction effect. Finally, the numerical findings are validated experimentally in the last section.

A. Introduction to OTR Liners Noise Reduction Mechanism

Before analysing the back reaction mechanism in the OTR liners, we present a brief overview of the different noise reduction mechanisms involved in the OTR liners. In the previous analytical work of OTR liners in ducts (Palleja-Cabre *et al.*, 2022b), the noise reduction mechanism was categorised into two types: (1) the noise *attenuation* caused by the acoustic energy dissipated by the liners, and (2) the *source modification* due to the back-reaction effects on the source due to the lined or hard-wall. It was also found that back-reaction effects on the source power are influenced by the proximity of the source to an impedance discontinuity. This effect is investigated further in this section. An attempt to qualitatively quantify the different noise reduction mechanisms was performed experimentally in (Palleja-Cabre *et al.*, 2020) by investigating the reductions in tip leakage noise in the presence of the OTR liners. Four different liner treatments were tested, which are shown in the schematic in Figure 7 (a). The same four boundary conditions are simulated here in the COMSOL Multiphysics. Through this study, it was found that a liner length close to 150 mm was sufficient to provide approximately 90% of the insertion loss compared to an infinite liner. The insertion loss increased marginally with further increase in the liner length beyond 150 mm. Hence, the length of the lined section for the OTR configuration was fixed at 150 mm. For consistency purpose, the lined boundary was extended by an equal length of 150 mm on either side of the OTR liner providing a full liner configuration of 450 mm. For the remote liner configuration the OTR configuration was reversed, thereby, the length of the lined section was 150 mm on each side of a 150 mm hard wall section, keeping the total section length constant at 450 mm. A hardwall boundary condition is imposed beyond the liner section, constituting a finite length liner. The source is located at a tip gap e of 0.01 m, which is in the region of back reaction for the frequencies tested here based on Figure 3. The source is fixed at this location to distinguish the role of the back reaction effect on the noise reductions. The insertion loss spectra in the far field is plotted against for different liner configurations in Figure 7 (b).

It can be seen in Figure 7 (b) that both the OTR liner and the full liner provide maximum noise reductions close to their resonance frequency of 2250 Hz. It is expected that the OTR liner, being only of a short length, would not be capable of providing significant levels of noise attenuation in the conventional sense of acoustic energy dissipated by the liner. However, since it is installed close to the source, it should be capable of providing source modification effects. A comparison of the predicted insertion loss for the OTR and full liner cases indeed suggests that the conventional attenuation effect is minimal for the OTR liner since the full liner only provides some 1-2 dB of additional insertion loss. Conversely, the noise reduction with the remote liner is weak across all frequencies. The remote liner configuration is expected to reduce noise mainly due to conventional attenuation and provide barely any back-reaction effects since the liner is located further away from the source. The results in Figure 7 (b) therefore suggest that the noise reductions in the OTR and full liner configurations are mainly driven by the source modification mechanism, which is being shown for the first time in this paper. In addition to the source modification and conventional attenuation mechanism, the discontinuity in the impedance boundary between the liner and the hard wall boundary might produce some back-scattering effects. The excess noise reduction with

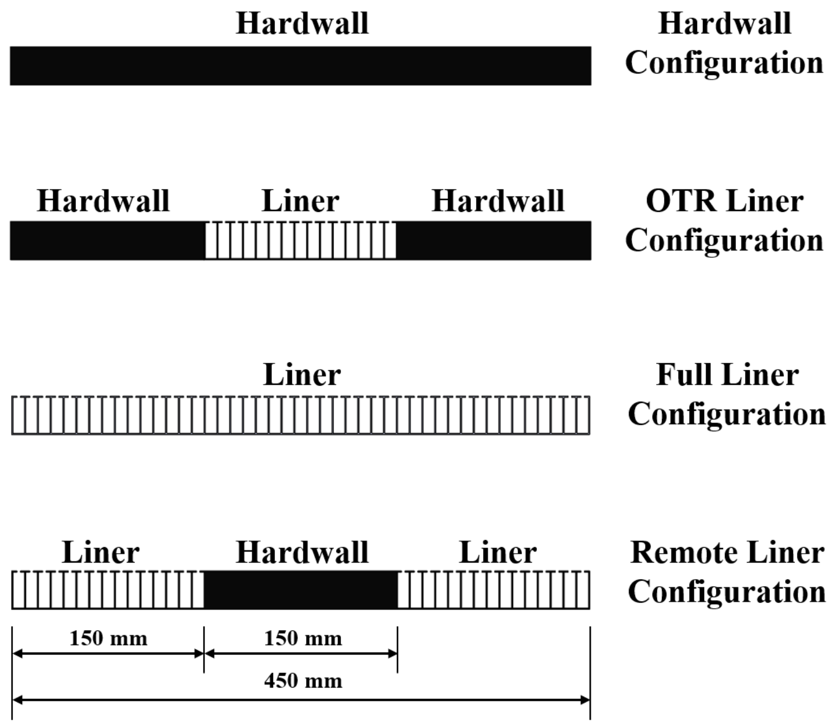

(a)

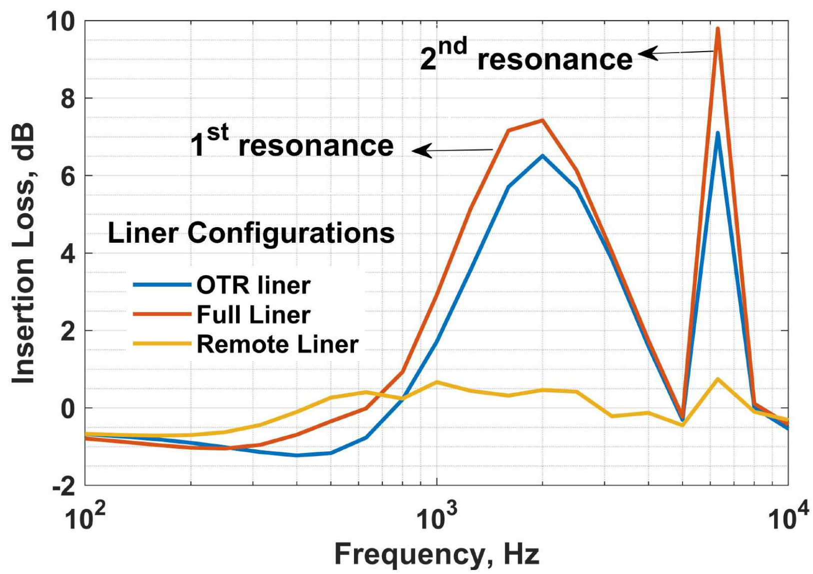

(b)

FIG. 7: (a) Boundary condition used in the experimental study, (b) Insertion loss variation with liner configurations.

the full liner compared to the OTR liner can also be the result of the conventional attenuation in the extended length of the liner and different back-scattering effects due to having the impedance discontinuity further away from the source. These however seem to be small in comparison to the source modification effects for this configuration. In conclusion, Figure 7 (b) indicates that a small length of the liner covering the region acoustically close to the source is sufficient to yield significant levels of noise reduction, which are predominantly caused by the source modification mechanism. This is another significant finding in this paper which is investigated further with the analysis of the acoustic particle velocity into the liner cavities in the upcoming section.

1. Role of the resonance condition of the liner on the Source Modification

In the previous section, the maximum noise reduction was analysed only at the resonance frequency of the liners. The dependency of source modification on the resonance condition is investigated here by calculating the power around the point source over a small circular region of 1 mm radius around the source, as shown in figure 8 (a). The acoustic power was calculated at five frequencies, covering the first two resonance, anti-resonance and a partial-resonance region. The frequencies of 2250 Hz and 7000 Hz are the resonance condition, 200 Hz and 5000 Hz are the anti-resonance, and 9400 Hz is partial resonance (0.5 absorption coefficient) for the considered liner. The normalised resistance and reactance (only the wire-mesh face sheet component) was defined at the boundary condition from the spectra shown in Figure 2. For comparison, the power in decibels (with an arbitrary reference of 1 dB) for each boundary condition is plotted against frequency in Figure 8 (b).

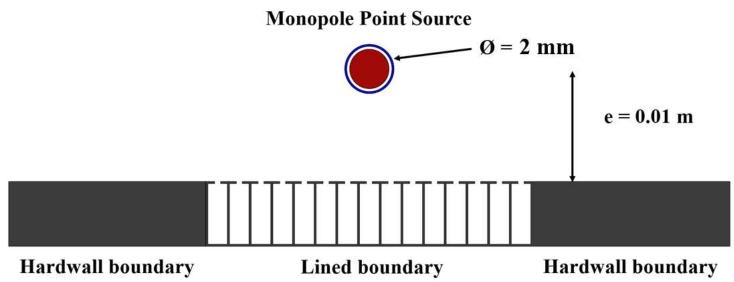

(a)

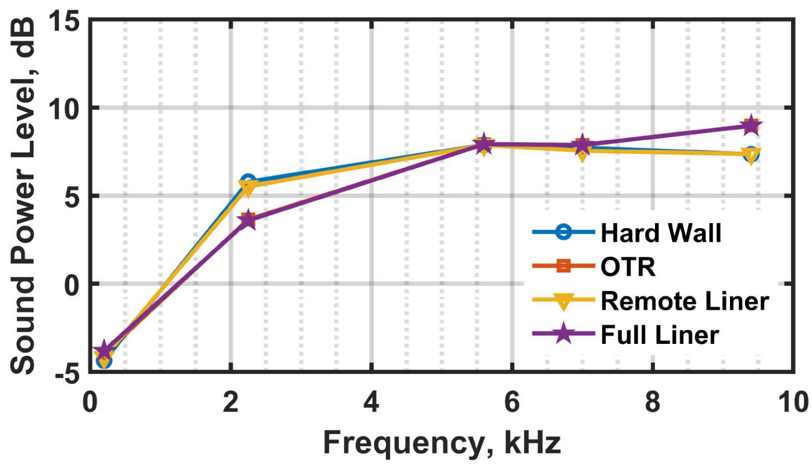

(b)

FIG. 8: (a) Schematic of the circle around the source defined in COMSOL, (b) Power around the source for different boundary condition.

It is clear from Figure 8 (b) that the remote liner has little effect on the source power as it shows the similar values of power output as in the case of a hard wall hard wall at all these frequencies. In contrast, the OTR liner and the full liner have reduced the source power in the resonance frequency by 4 dB. In fact, both these boundary conditions have a similar effect on the source, which shows again that the small liner length is sufficient to have the maximum reduction in source power. This short length of the liner is where the source modification due to the back reaction effect is expected to be dominant. At frequencies of 7000 Hz and 9400 Hz, which are resonance and partial resonance respectively, a slight increase in the power around the source is observed, which could be the effect of the scattering at the impedance discontinuities. At the anti-resonance frequencies, all boundary conditions show identical results as they are effectively a hard wall condition. This signifies that the source modification effect is dependent on the resonance condition. Nevertheless, it is difficult to argue that the source modification is the sole reason for the increased noise reduction achieved with the OTR liner as back scattering effects also affect the radiated noise, which will be analysed in the subsequent section.

2. Mechanism of source modification

Source modification is one of the dominant mechanisms of noise reduction achieved with the OTR liners as shown by the analysis in the previous section. However, this section is focused on explaining the physical mechanism of the source modification. It was shown that the source modification effects are dominant at the resonance frequencies. This observation led to the evaluation of the acoustic particle velocity flowing into the liner when the noise is generated at the resonance and anti-resonance frequencies of the liner. The vertical component of the particle velocity over each cavity is integrated over the liner length to determine the volume flow or the source strength on the liner surface. The resonance frequency of 2250 Hz and anti-resonance frequency of 200 Hz are used for this analysis.

The vertical velocity contours for the frequencies of 2250 Hz and 200 Hz are presented in Figures 9 (a) and (b) respectively. Additionally, in Figure 10, the volume flow rate measured along the liner surface on either side of the source for tonal excitation at the resonance (2250 Hz) and anti-resonance (200 Hz) frequency is shown. From the velocity contour plot for the resonance frequency 9 (a), a peak can be seen in the acoustic particle velocity flow over the liner surface directly near the source location. A similar trend in the volume flow rate is also observed, as shown in the Figure 10, where the maximum volume flow rate is at the centre of the liner length. The volume flow rate drops gradually with the distance away from the centre. This peak resembles a source formation with out of phase compared to the primary monopole source.This is verified with the contour of the phase of the acoustic pressure shown in Figure 11 (a). As seen in the phase plot, the acoustic pressure in the liner is out of phase with the sound pressure outside the cavities. It is also noted that the strength of this secondary source is comparable to the primary monopole source. However, at the anti-resonance condition, as shown in Figure 10, the magnitude of the velocity flow in the liner is minimal since the liner behaves like a hard wall. The source formation is therefore also limited in the anti-frequencies given by Figure 9 (b). Correspondingly, there is no change in the phase of the sound pressure as shown by the phase contour in Figure 11 (b). This analysis implies that the source modification could be the result of the interference between the primary monopole source and a secondary source on the liner surface caused

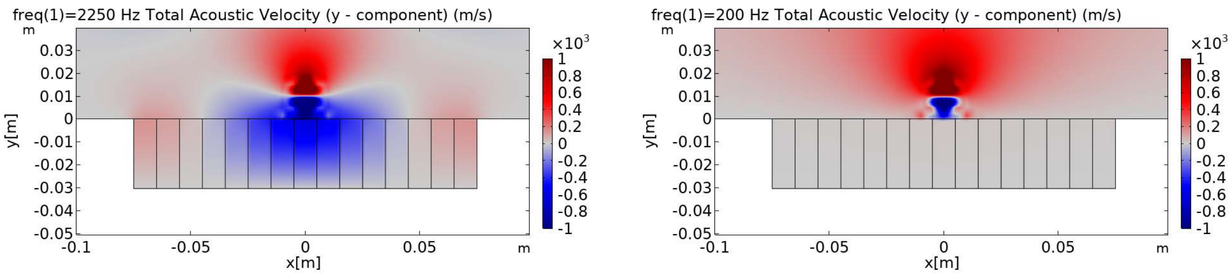

(a)

(b)

FIG. 9: (a) Velocity contour (y - component) in the liner at resonance frequency of 2250 Hz, (b) Velocity contour (y - component) in the liner at anti-resonance frequency of 200 Hz.

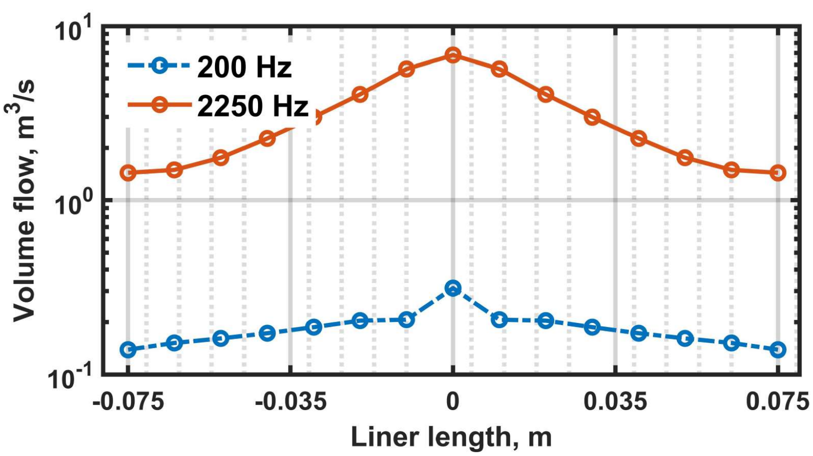

FIG. 10: Comparison of volume flow rate into the liner cavity at the anti - resonance and resonance frequency.

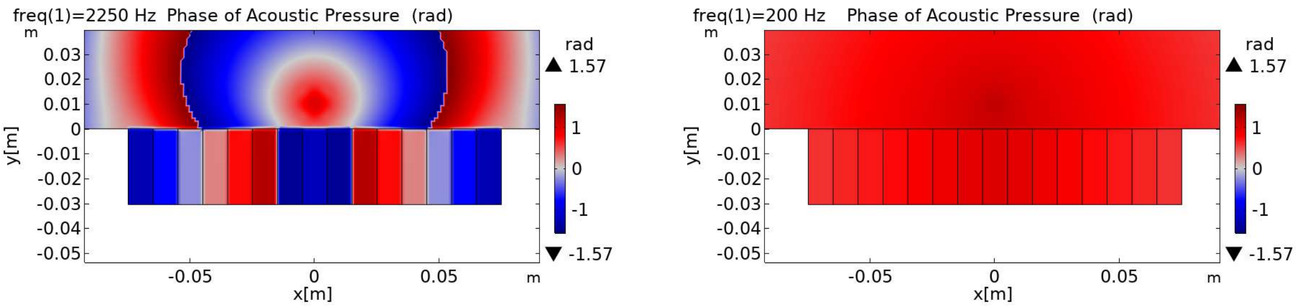

(a) (b)

FIG. 11: (a) Phase of the acoustic pressure (y - component) for 2250 Hz, (b) Phase of the acoustic pressure (y - component) for 200 Hz.

by the increase in the particle velocity flow at the resonance frequency of the liner which resembles an image source formation on the liner surface.

To further verify the influence of the liner resonance condition on the source modification effect, the liner is now intentionally tuned to be in resonance at a frequency of 200 Hz by increasing the cavity depth from 30.48 mm (tuned for resonance at 2250 Hz) to 429 mm. The volume flow rate and the velocity contour with the modified cavity depth are shown in Figure 12. There is an increase in the velocity flow when the liner is tuned for 200 Hz compared to the previous case for the same excitation frequency. This clearly shows that the image source formation on the liner surface is the strongest when the monopole excitation frequency matches to the liner resonance frequencies. This secondary source has a destructive interference with the primary noise source, as shown by the phase of the acoustic pressure in Figure 11 (a) and (b), thereby reducing the efficiency of noise radiated.

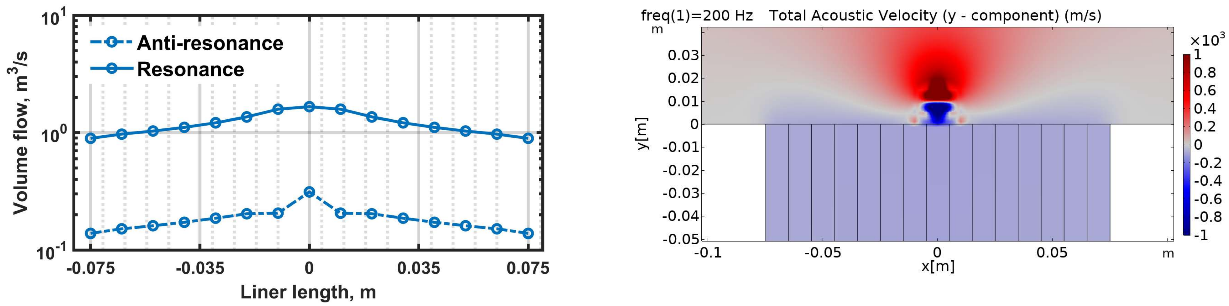

(a) (b)

FIG. 12: (a) Volume flow rate into the liner tuned for 200 Hz, (b) Velocity contour (y - component) with liner tuned for 200 Hz.

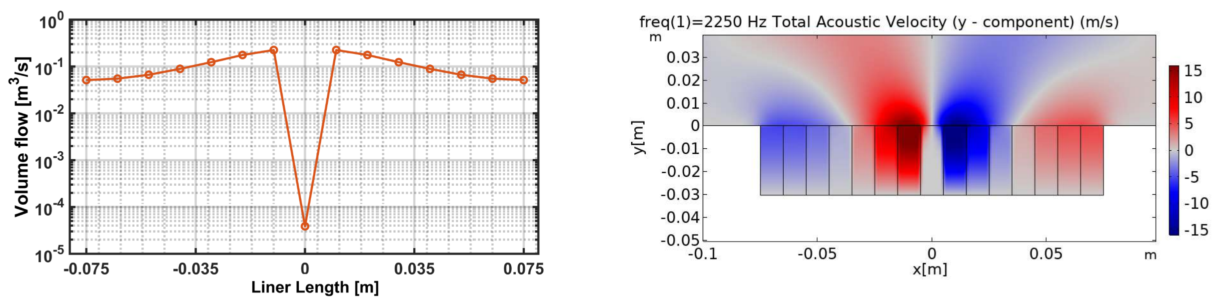

(a) (b)

FIG. 13: (a) Volume flow rate into the liner cavity with a dipole source at resonance frequency of 2250 Hz, (b) Velocity contour (y - component) with dipole source at resonance frequency of 2250 Hz.

The model was extended to a horizontal dipole source of the same strength. The results for this case are shown in Figure 13, which shows a dipole source formation on the liner surface. This observation is supported by the volume flow rate plot in Figure 13 (a), in which two peaks can be observed with a drop in the volume flow at the centre of the liner. This drop corresponds to the directivity of the dipole source as shown in Figure 13 (b). The phenomenon of secondary source formation on the OTR liner surface, for condition when the liner is at resonance, is being shown for the first time in this paper. This phenomenon is hypothesised as the key mechanism of source modification in the OTR liners, and it is independent of the noise source strength.

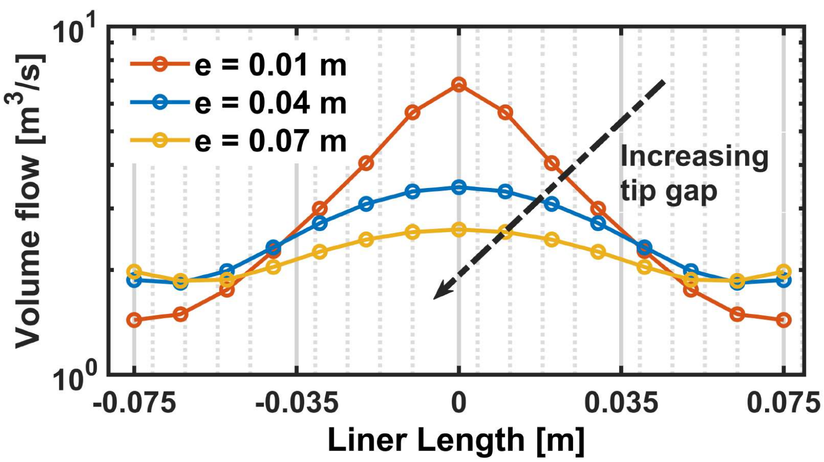

FIG. 14: Comparison of volume flow rate into the liner at resonance frequency of 2250 Hz for different tip gaps.

The effect of the tip gap on the source modification effect is also investigated by varying the tip gaps to 0.04 m and 0.07 m. In Figure 14, the volume flow rate is plotted against the liner length for varying tip gaps. It can be observed from the figure that there is a decrease in the volume flow rate into the liner when the tip gap is increased. The volume flow rate at the tip gap of 0.04 m is half of the volume flow rate at the tip gap of 0.01 m whereas for the 0.07 m tip gap the volume flow rate is reduced approximately by 0.8 m^3/s compared to the tip gap of 0.04 m. This marginal difference in the volume flow rate beyond 0.04 m is an indicator of the decrease in the significance of the source modification effect. This observation is in agreement with the analytical optimal impedance result in Figure 3 that the tip gap of 38 mm or $e/\lambda = 0.25$ could effectively be the transition point where the source modification effect becomes weaker.

3. Back Scattering effects in the finite OTR liner

Figure 15 (a) shows the directivity of the sound pressure levels for the OTR liner configuration (see Figure 7 (a)) with a monopole source located at a tip gap, e of 0.01 mm and excited at different tonal frequencies, between 200 Hz and 9400 Hz. In the OTR liner configuration the liner length is set to 0.15 m, representing the experimental conditions. The directivity of the sound pressure level was estimated at a radial distance of 4.5 m in the model for every 10° angle. As it can be seen from Figure 15 (a), when the source is excited at the anti-resonance of the liner (200 Hz and 5600 Hz), there is not much difference in the directivity patterns. This is expected since the liner impedance in those conditions is effectively that of a hard wall case mainly due to a normalised reactance (X) that tends to infinity.

However, when the liner is at resonance (2250 Hz and 7000 Hz), there is a significant drop in noise level at angles between $20° - 60°$ and $120° - 160°$ compared to the anti-resonance

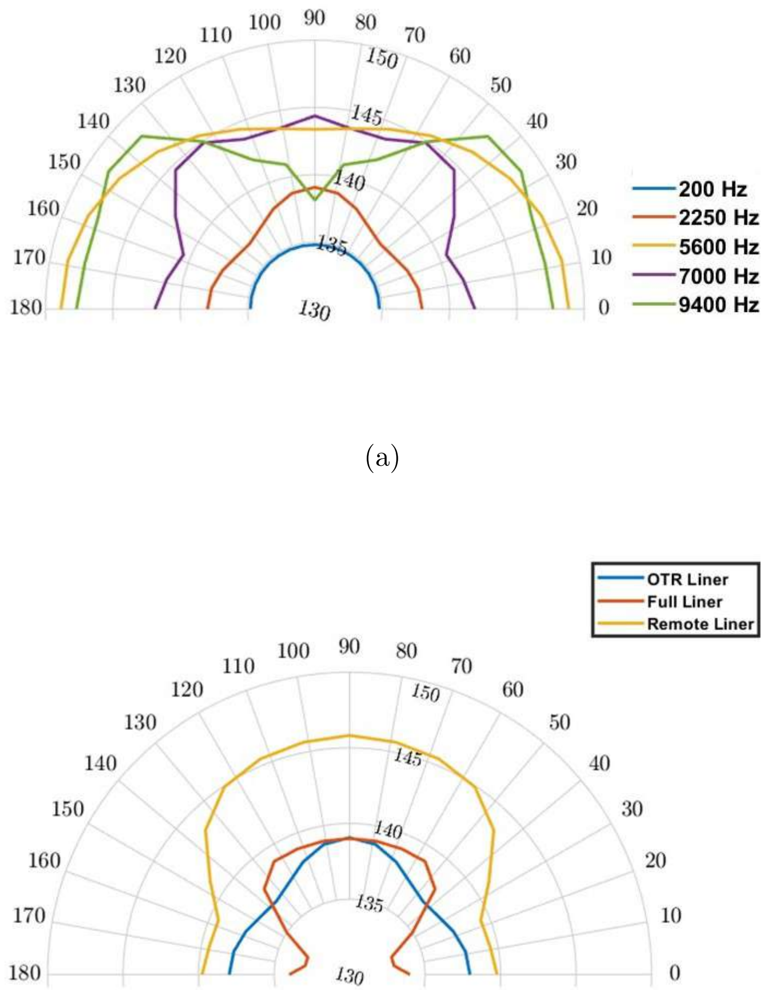

(a)

(b)

FIG. 15: (a) Directivity variation with frequency, (b) Directivity variation with liner length at resonance.

condition. Also, at partial resonance condition (9400 Hz), the noise level is dropping only between $45^{\circ} - 135^{\circ}$. The observed changes in the directivity can be attributed to

- the discontinuity in the impedance around the lined section edges (see Figure 5), mainly the normalised reactance (X) of the liner, which changes from $X = 0$ at resonance to $X = \infty$ at anti-resonance in the promixity of the sound source, and
- the significant change in the phase of the acoustic pressure (see Figure 11 (a)) at resonance compared to the anti-resonance (see Figure 11 (b)).

Both can cause destructive interference between the incident and reflected waves from the edges of the liner length, which we refer here as "Back scattering effect".

Figure 15 (b) shows the directivity pattern for different liner configurations (see Figure 7 (a)) at the 2250 Hz resonance frequency. The noise level with the remote liner configuration is far higher compared to the full liner or the OTR liner configurations. A 7 dB difference in the noise level between the remote liner and the full liner can be observed for the angles between $60° - 90°$. Since the source modification effect is absent in the remote liner, this difference in the noise level is expected. Comparing the directivity of the full liner with the OTR liner, the maximum noise level is identical between $80° - 100°$. In addition, there is a drop in the noise level between the $105° - 30°$ and $150° - 170°$. As the source modification effect is similar with both the full liner and OTR liner, this increase in the noise reduction with a full liner could be the result of the scattering variation with liner length and the increase in the absorption of the liner. However, as shown in the earlier sections, within the region of $e/\lambda < 0.25$, the absorption effect of the liner is minimal hence, the variation in the back scattering could be the main reason for the drop in the noise level. The noise reduction with the OTR liner is therefore due to the combination of source modification due to the back reaction, conventional attenuation, and back scattering due to the impedance discontinuities around the liner edges. As the liner length modifies the back scattering, the insertion loss also changes with the liner length, which is investigated numerically in the next section.

B. Numerical optimal impedance study on finite liners

The analytical results of the optimal impedance study in section II.A did not account for the back scattering effects as the analytical model assumes that the source is placed in the proximity of an infinitely lined plane. As a result, in this section we investigated if the back scattering effects are likely to modify the optimal impedance. The numerical optimal impedance was determined by varying the resistance between 0 to $3\rho c_0$ with the resolution of $0.25\rho c_0$ and the reactance between $-3\rho c_0$ to $+3\rho c_0$ with the resolution of $0.5\rho c_0$. The optimal impedance was also calculated for different cases of liner lengths to identify the point where the 'infinite liner' behaviour begins approaching the analytical solutions. In this study, two tip gaps were considered;

- in the first case, the point source was positioned in the region of back reaction ($e/\lambda < 0.25$), and
- in the second case, the point source was positioned in the region of absorption close to the transition point.

For the resonance frequency of 2250 Hz, these corresponds to the tip gaps of 0.01 m and 0.04 m with $e/\lambda = [0.066, 0.26]$ respectively.

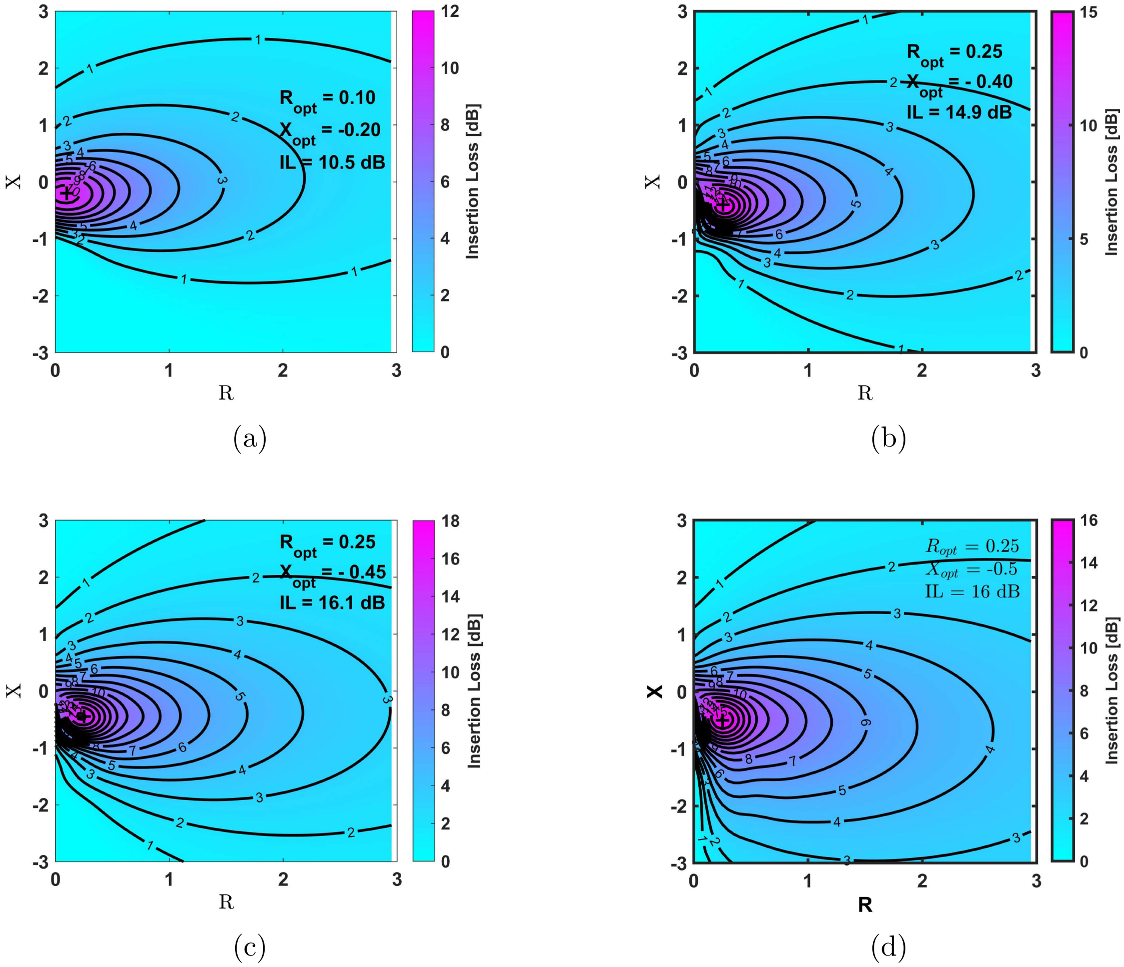

FIG. 16: Numerical optimal impedance contour at $e/\lambda = 0.066$ and (a) $L/e = 4$, (b) $L/e = 15$, (c) $L/e = 30$, and (d) $L/e = 900$.

For the case of $e/\lambda = 0.066$, four different liner lengths were considered $L/e = [4, 15, 30, 900]$. The numerical optimal impedance contour for the chosen liner lengths is shown in Figure 16. The overall comparison of the numerical and analytical results (Figure 4(a)) shows that the maximum insertion loss is far lower for the numerical model. This is expected as the numerical model considers a finite liner. The resistance values are also larger than the analytical model, correspondingly the source modification effects are reduced. In addition, the back scattering effects from the impedance discontinuities is further modifying the optimal impedance and the insertion loss depending on the length. Comparing the optimal impedance between different liner lengths, the resistance of the liner was found to increase when increasing L/e while the reactance of the liner gradually drops. However, for $L/e > 15$, we observe smaller changes in the insertion loss (IL) and optimal impedance, with a marginal change in reactance alone. The optimum reactance obtained with the numerical model is close to the value evaluated with the analytical model, as shown in Figure 4 (a). This effectively means that the back reaction is reaching its saturation point at $L/e = 15$. Extending the liner length beyond this value will only increase the absorption and modifies the scattering effects. This implies that for $e/\lambda = 0.066$ at 2250 Hz, the liner starts to behave as an infinite liner at $L/e = 15$, which is shown below.

The optimal impedance contour for $e/\lambda = 0.26$ is plotted for four different liner lengths with $L/e = [1, 3.75, 50, 225]$ in Figure 17. The variation of the resistance and reactance with the liner length is similar to the previous case of $e/\lambda = 0.066$. However, a significant aspect is that the insertion loss with the smaller liner of $L/e = 1$ is now 1 dB higher than for the case of the larger liner with $L/e = 3.75$. This can be due to the back scattering effect producing a constructive interference at $L/e = 1$ and destructive interference at $L/e = 3.75$ on the total sound field. Since the point source is located in the region of absorption, the back scattering effect is having a stronger influence on the insertion loss. This effect was negligible within the region of back reaction. Like in the previous case, the optimal resistance is not changing much after $L/e = 3.75$ but the reactance has decreased significantly. Beyond $L/e = 50$, the resistance and reactance changes are smaller and the

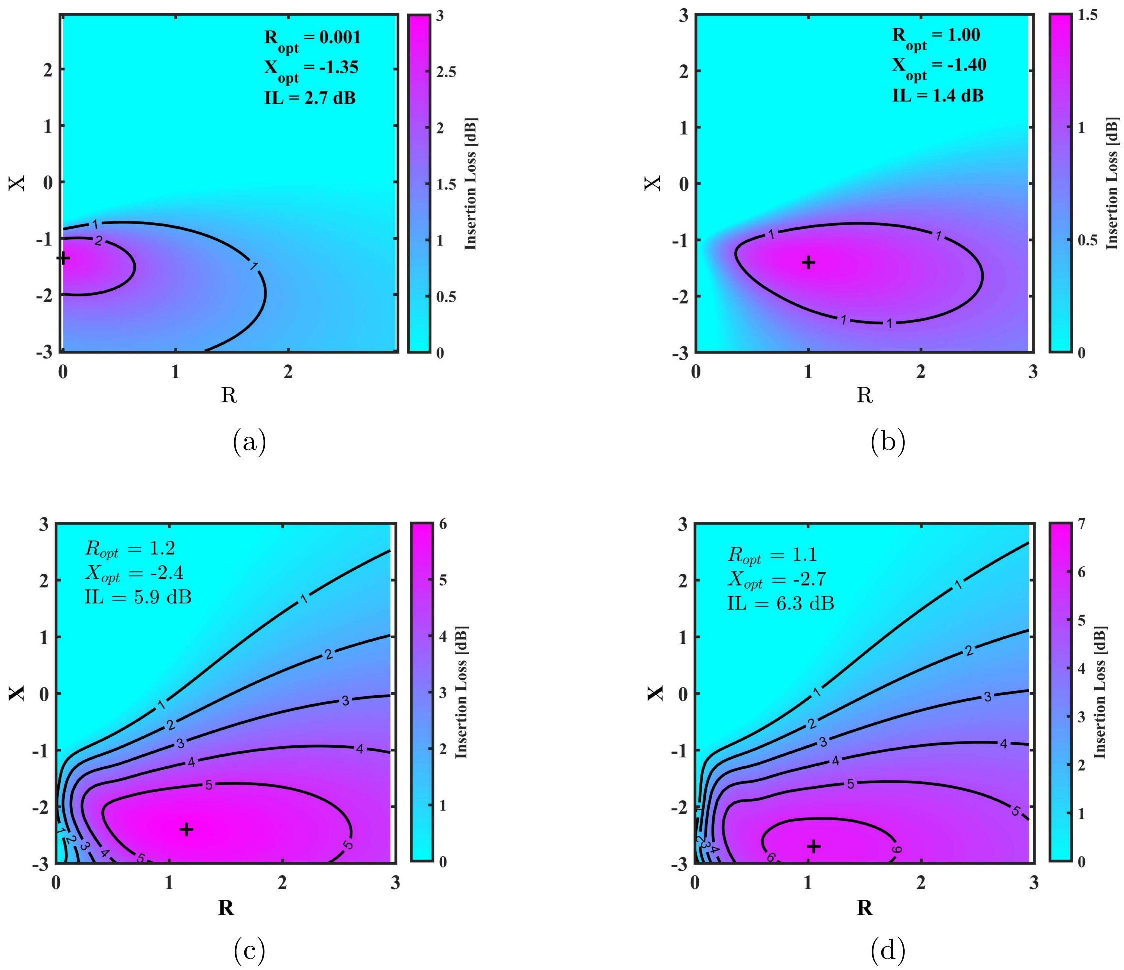

FIG. 17: Numerical optimal impedance contour at e/λ = 0.26 and (a) L/e = 1, (b) L/e = 3.75, (c) L/e = 50, and (d) L/e = 225.

reactance is again closer to the analytical model value in Figure 4 (b). So, the minimum required liner length for an 'infinite lined plane' behaviour for $e/\lambda = 0.26$ at 2250 Hz is therefore $L/e = 50$. As the considered tip gap is close to the transition point at this frequency, a larger liner length is required to exhibit the infinite liner behaviour. This also shows that outside the back reaction region, the relation between the liner length and the tip gap can not be generalised.

To formulate a non-dimensional relationship between the liner length, wavelength, and tip gap, the insertion loss for a specific tip gap and frequency is now evaluated. The insertion loss was calculated for the tip gaps $e = [0.01,\ 0.02,\ 0.04]$ m for the noise frequencies of 1000 Hz, 2250 Hz, and 4500 Hz. The liner was tuned in each case to be in resonance for the frequency of the source. The tip gaps and the frequencies were chosen in such a way as to assess the influence of the back reaction on the liner length. The selected tip gaps and frequency represent the region of back reaction, the transition point, and the region of absorption. It was observed earlier that the optimal impedance variation was minimal beyond $L/e = 15$ for the tip gap of $e = 0.01\ m$. The optimal impedance with $L/e = 15$ for each frequency 1000 Hz, 2250 Hz, and 4500 Hz is therefore used to evaluate the insertion loss. Similarly, the optimal impedance variation was found to be minimal after $L/e = 15$ for the 0.02 m tip gap as well and hence the insertion loss variation was calculated with the corresponding value. The tip gap of 0.04 m has $e/\lambda > 0.25$ except for the low frequency of 1000 Hz. Hence it was difficult to identify the liner length where the optimal impedance became constant. The results for $L/e = 15$ were however used to calculate the insertion loss in the comparison study. In Figure 18, the evaluated insertion loss is plotted against the liner length normalised by the respective tip gaps.

The overall comparison of insertion loss shows the drop in noise reduction with the increase in the tip gaps, in agreement with the earlier observations. For the tip gap of $e = 0.01\ m$ in the Figure 18 (a), the insertion loss curves flatten after the $L/e = 17$ for each of the frequencies. The sound source is located within the region of back reaction in all the considered frequencies for this tip gap. In contrast, for $e = 0.02\ m$ in Figure 18

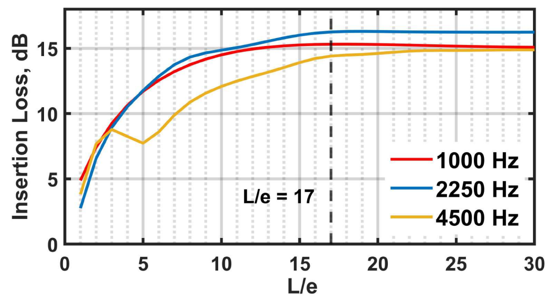

(a)

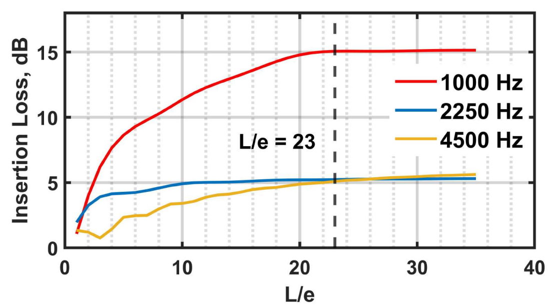

(b)

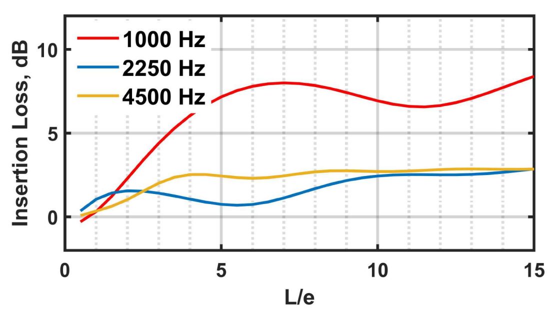

(c)

FIG. 18: Insertion loss variation with liner length for different frequencies at (a) $e = 0.01\ m$, (b) $e = 0.02\ m$, and (b) $e = 0.04\ m$.

(b), the insertion loss becomes constant close to $L/e = 23$. The sound source is at the transition point at 4500 Hz for this tip gap while it is in the back reaction region for the other two frequencies. For the case of 0.04 m tip gap in Figure 18 (c), the sound source is in the region of back reaction, transition point and at the region of absorption at frequencies 1000 Hz, 2250 Hz, and 4500 Hz respectively. Though the insertion loss looks to be constant beyond $L/e = 10$ at 2250 Hz and 4500 Hz, it is yet to attain a constant value for 1000 Hz. The insertion loss is also marginally higher at 4500 Hz than 2250 Hz despite the tip gap being in the region of absorption in the former frequency. This is attributed to the back scattering having a constructive interference on the noise reduction.

Another feature to be noted in Figure 18 is that the maximum insertion loss has shifted towards the lower frequencies of noise as the tip gap is increased. This is because the back reaction effect is dominant only in the region $e/\lambda < 0.25$. When the tip gap is increased while keeping the frequency and hence, the wavelength constant, the e/λ ratio increases. Then, the noise source is no longer present in the region of back reaction in the considered frequency. However, when the frequency is reduced simultaneously while increasing the tip gap such that the $e/\lambda < 0.25$, the noise source will still be in the region of back reaction.The maximum noise reduction will therefore shift to lower frequencies as the tip gap is increased. However, the liner length required to yield such levels of noise reduction also increases at these larger tip gaps. This trend was observed while verifying the model, where a longer liner was required to improve the noise reduction in the lower frequency. It is further shown by the increase in the minimum L/e ratio when the tip gap is increased from 0.01 m to 0.02 m in Figure 18. Accordingly, for the tip gap of 0.04 m, the insertion loss will saturate at a larger L/e value and at a much lower frequency. This shows that in the back reaction region, there is an interlinkage between the tip gap, the frequency of the source, and the liner length, which determines the optimal impedance of the OTR liner. Hence, the optimum normalised liner length, L/e to obtain the maximum noise reduction cannot be generalised unless the tip gap and the frequency of the noise are fixed. However, it is shown conclusively that to obtain maximum back reaction effects, only a small length of the liner is sufficient. This indicates that the OTR liner can be designed to provide maximum noise reduction with an optimal liner length.

C. Experimental Validation

This section presents a validation of the numerical results found in the previous analysis with experimental data. The experiment was performed in the anechoic chamber at the ISVR with a loudspeaker source effective for a range of frequencies from 500 Hz to 6500 Hz. A tube of 20 mm diameter was attached to a loudspeaker to produce a plane wave propagation in the tube (approximately up to 10 kHz). Therefore, the sound emitted from the unflanged pipe would radiate with a transmission coefficient $(\tau_{\Pi}) \approx (ka)^2$, and can be treated as a monopole source radiation (Kinsler *et al.*, 1999). The experimental test setup is shown in Figures 19 (a). An SDOF liner with a cavity depth of 30.48 mm was used. The source was located above the centre of the liner panel. The impedance was varied by considering open cavities and a wiremesh facing sheet. A tonal noise of 2250 Hz (resonance) and 5600 Hz (anti-resonance) frequency was generated and the gap between the source and the liner was varied in steps of 5 mm between 5 mm and 55 mm, and then in steps of 20 mm up to

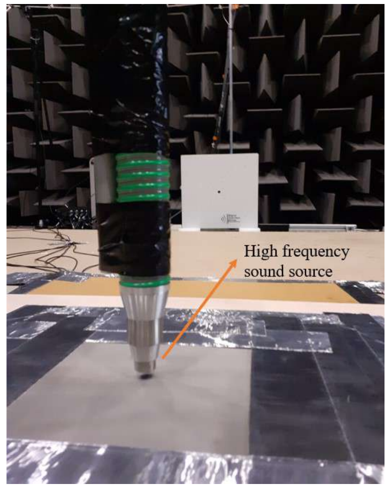

(a)

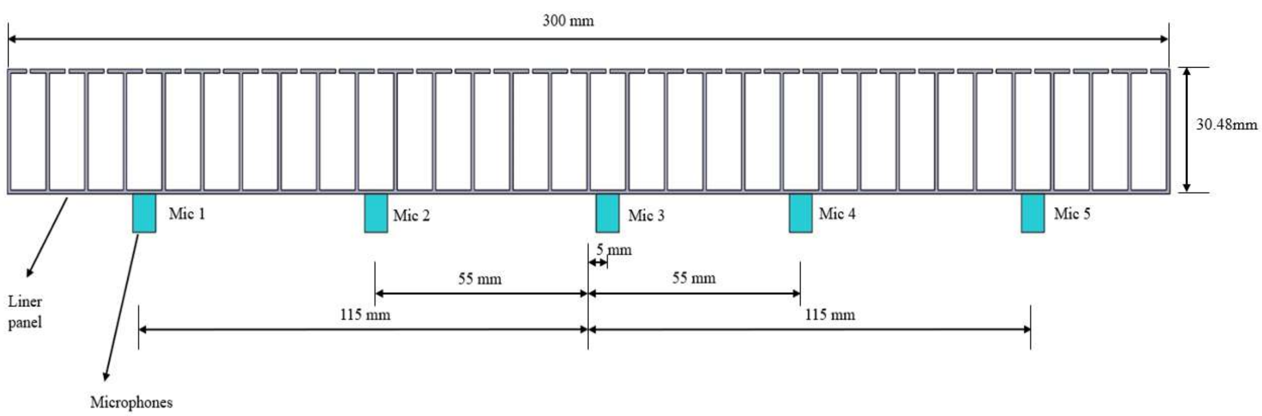

(b)

FIG. 19: (a) Sound source over a lined wall, and (b) Surface pressure microphones in the backing sheet of the liner panel.

115 mm. The surface pressure in the backing sheet of selected liner cavities was measured to validate the source modification mechanism. Five quarter-inch condenser microphones were mounted in the backing sheet of the liner at 5 mm, 55 mm and 115 mm on either side of the source for this measurement as showcased in Figure 19 (b).

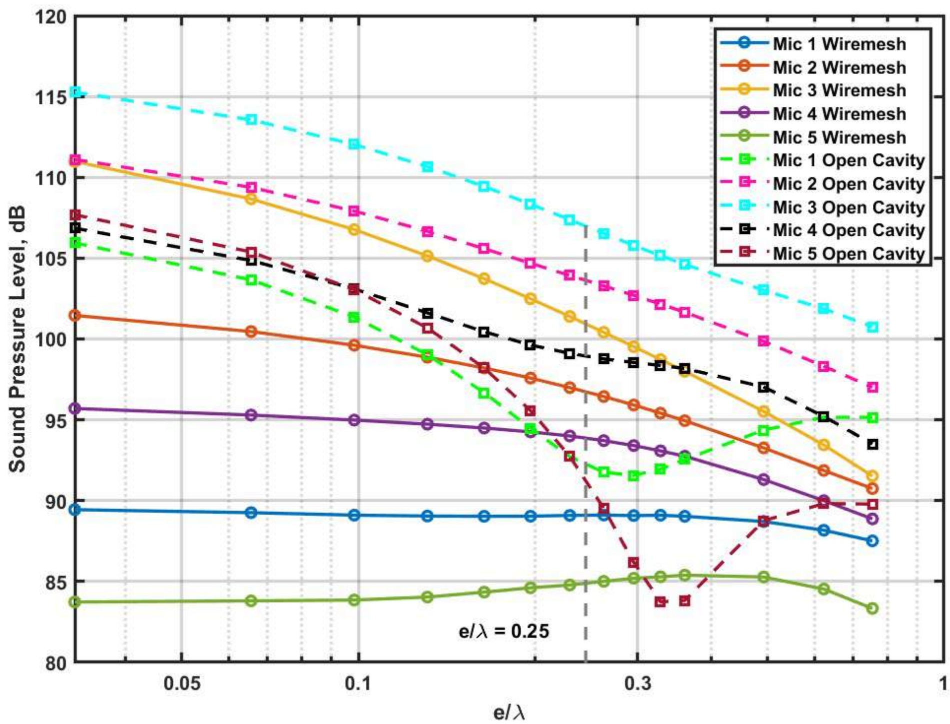

FIG. 20: Comparison of Sound Power Level inside the cavity for different impedance conditions at 2250 Hz.

The surface pressures measured in the cavities are presented in terms of the Sound Pressure Level (SPL) against the normalised tip gap in Figure 20 for a frequency of 2250 Hz. The measurements taken with a wiremesh liner are shown by the solid lines and those for the open cavity liner by the dashed lines. As expected, the open cavity liner has a higher sound power level in the cavities due to the higher particle velocity flow compared to the wiremesh liner. It can also be observed that the cavities closer to the centre have maximum SPL values, as shown by Mic 2, Mic 3, and Mic 4. This implies that the particle velocity flow is stronger in the cavities closer to the source, providing maximum source modification effects. This is expected and agrees with the numerical results that show that the cavities closer to the source were more active. This also supports the conclusion that a small length of the liner is enough to yield maximum source modification effects.

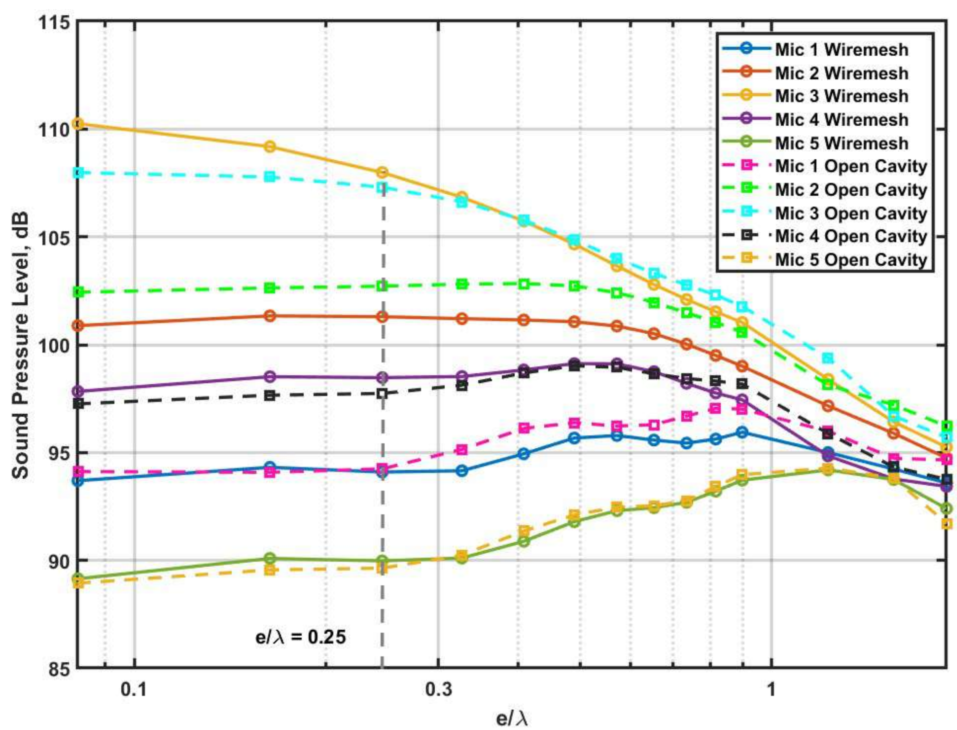

FIG. 21: Comparison of Sound Power Level inside the cavity for different impedance condition at 5600 Hz.

The SPL in the cavity for 5600 Hz in Figure 21 shows that both liners perform similarly at this frequency, as it is the anti-resonance condition. In comparison to the case at 2250 Hz, there is a 7 dB to 10 dB drop in the power level for the open cavity liner. However, the power level for the wiremesh liner drops only by 2 dB to 3 dB.

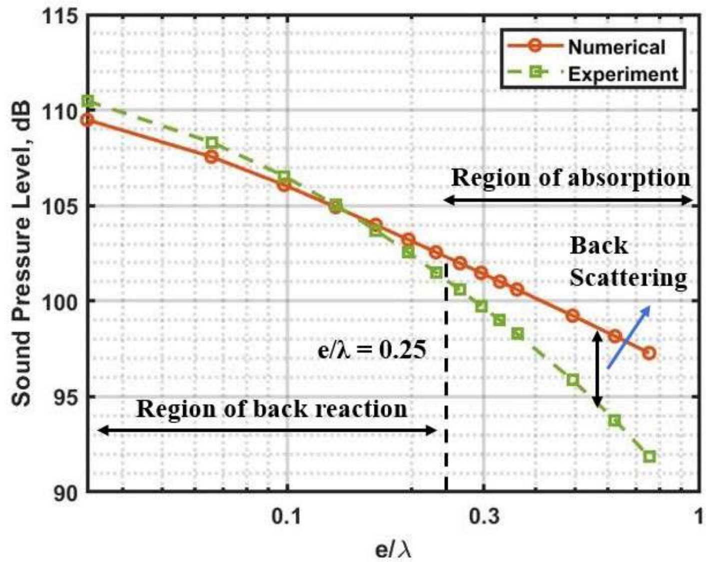

FIG. 22: A comparison of numerical and experimental sound pressure level at the backing sheet of the centre cavity for a tonal excitation at 2250 Hz (resonance) and the tip gap varying between 5 mm and 115 mm.

Finally, the SPL in the backing sheet of the centre cavity of the liner was determined numerically for various tip gaps at the resonance frequency. The numerical data is compared with the experimental results with a wiremesh facing sheet in Figure 22, which are found to be in good agreement in the region of back reaction ($e/\lambda < 0.25$). Some deviations are observed in the region of absorption at the larger tip gaps, with the predicted values showing larger sound levels than the experimental data. Nevertheless, the general trends observed with the numerical model can also be seen in the experimental results, which confirms the validity of the numerical model developed in the current study.

IV. CONCLUSION

This paper presents a numerical investigation of the noise reduction performance of acoustic liners placed over or close to a sound source. This fundamental study was performed to improve the understanding of the noise reduction mechanisms in OTR liners in the absence of a background flow. Thereby, the noise reduction mechanisms in the OTR liners are explained purely from an acoustical point of view. The problem is modelled in COMSOL multiphysics with a static point source placed over a finite lined panel in a half-plane domain. A parametric study for different liner configurations is performed by evaluating the insertion loss of the liners, their effect on the noise directivity, and the particle velocity across the liner facing sheet. Additionally, the numerical results and observations in the paper are validated through an experimental study.

The results of the numerical investigation indicate that the noise reduction in OTR liners is a combination of source modification, back-scattering due to the impedance discontinuities between the liner and the hardwall, and the conventional absorption of the liner. One of the key findings of this paper is the explanation of the underlying physics of the source modification mechanism in OTR liners. This effect was hypothesised in the literature as the primary noise reduction mechanism in OTR liners. The source modification is identified to be most effective in reducing the noise when the excitation frequency is close to the resonance frequency of the liner. In such conditions, the acoustic particle velocity flow at the liner surface is found to be maximum and acts as a secondary source that is out of phase with respect to the primary source. The interference between this secondary source and the primary sound source is conceptualised as the back reaction or source modification effect in OTR liners.

An optimal impedance study at the resonance frequency of the liner has shown that the source modification effects due to the back reactions are dominant for non-dimensional tip gaps $e/\lambda < 0.25$. It is also shown that the liner length can be optimised within this region ($e/\lambda < 0.25$) to provide maximum insertion loss with only a small treated insert of normalised liner length L/e immediately below the source. Back scattering effects are found to be most significant in the region of $e/\lambda > 0.25$, which complicates the determination of an optimal liner length in such conditions. The optimal impedance and maximum insertion loss are found to be a function of the tip gap, the liner length, and the acoustic wavelength.

This work represents an initial step in understanding the working principle of OTR liners in the absence of flow. It provides guidelines for the design of OTR liners in engineering applications and an explanation of the underlying physics of the acoustic source modification mechanism in OTR liners. However, the observed mechanism is likely to be impacted by the flow field, which might in turn be modified by the presence of the OTR liners. The liner behaviour and the duct propagation at high sound pressure levels will also influence the mechanism of OTR liner noise reduction. These effects are however outside the scope of the current work and will be investigated in future studies.

ACKNOWLEDGMENTS

This work has received funding from the Royal Academy of Engineering (RF\201819 \ 18 \ 194). The authors also wish to acknowledge the continuing support provided by Rolls–

Royce plc through the University Technology Centre in Propulsion Systems Noise at the Institute of Sound and Vibration Research.

Reference

Bozak, R., and Dougherty, R. P. (**2018**). "Measurement of Noise Reduction from Acoustic Casing Treatments Installed Over a Subscale High Bypass Ratio Turbofan Rotor," in *AIAA/CEAS Aeroacoustics Conference*, 4099, https://arc.aiaa.org/doi/10.2514/6.2018-4099, doi: 10.2514/6.2018-4099.

Bozak, R., Hughes, C., and Buckley, J. (**2013**). *The aerodynamic performance of an over-the-rotor liner with circumferential grooves on a high bypass ratio turbofan rotor*, **55225** (American Society of Mechanical Engineers).

Ingard, U. (**1951**). "On the reflection of a spherical sound wave from an infinite plane," The Journal of the Acoustical Society of America **23**(3), 329–335.

Jones, M., Parrott, T., Sutliff, D., and Hughes, C. (**2009**). "Assessment of soft vane and metal foam engine noise reduction concepts," in *15th AIAA/CEAS Aeroacoustics Conference (30th AIAA Aeroacoustics Conference), 11 - 13 May, Miami, Florida*.

Kinsler, L. E., Frey, A. R., Coppens, A. B., and Sanders, J. V. (**1999**). *Fundamentals of Acoustics*, 4th ed. (John Wiley and Sons Inc.).

Levine, H. (**1980**). "Output of acoustical sources," The Journal of the Acoustical Society of America **67**(6), 1935–1946.

Palleja-Cabre, S., Tester, B. J., Astley, J., and Bampanis, G. (**2020**). "Aeroacoustic assessment of the performance of over-tip liners in reducing noise of an aerofoil over a flat surface," in *AIAA AVIATION 2020 FORUM, 15 - 19 June, AIAA 2020-2608*.

Palleja-Cabre, S., Tester, B. J., and Astley, R. J. (**2022**a). "Modeling of Over-Tip-Rotor Liners for the Suppression of Fan Noise," AIAA Journal **60**(11), 6361–6373, doi: 10.2514/1.J061661.

Palleja-Cabre, S., Tester, B. J., and Astley, R. J. (**2022**b). "Modelling of ducted noise sources in the proximity of acoustic liners," Journal of Sound and Vibration **517**, 116548.

Sun, Y., Wang, X., Du, L., and Sun, X. (**2022**). "On the flow-acoustic coupling of fan blades with over-the-rotor liner," Journal of Fluid Mechanics **941**, 1–35, doi: 10.1017/jfm.2022.323.

Sutliff, D., Elliott, D., Jones, M., and Hartley, T. (**2008**). "Collaboration with williams international to demonstrate the characteristics of a foam-metal-liner installed over-the-rotor of a turbofan engine," in *Acoustics Technical Working Group Meeting*, E-16781.

Sutliff, D., Elliott, D., Jones, M., and Hartley, T. (**2009**). "Attenuation of fj44 turbofan engine noise with a foam-metal liner installed over-the-rotor," in *15th AIAA/CEAS Aeroacoustics Conference (30th AIAA Aeroacoustics Conference), 11 - 13 May, Miami, Florida*.

Sutliff, D. L., and Jones, M. G. (**2009**). "Low-speed fan noise attenuation from a foam-metal liner," Journal of aircraft **46**(4), 1381–1394.

Thomasson, S.-I. (**1976**). "Reflection of waves from a point source by an impedance boundary," The Journal of the Acoustical Society of America **59**(4), 780–785.